ChemPubSoc Europe

DOI: 10.1002/chem.201902794

CHEMISTRY A European Journal Full Paper

Cluster Compounds

Non-covalent Interactions and Charge Transfer between Propene and Neutral Yttrium-Doped and Pure Gold Clusters

Júlia Barabás,[d] Jan Vanbuel,[b] Piero Ferrari,[b] Ewald Janssens,*[b] and Tibor Höltzl*[a, c, d]

Abstract: The dopant and size-dependent propene adsorption on neutral gold (Au_n) and yttrium-doped gold ($Au_{n-1}Y$) clusters in the $n = 5$–15 size range are investigated, combining mass spectrometry and gas phase reactions in a low-pressure collision cell and density functional theory calculations. The adsorption energies, extracted from the experimental data using an RRKM analysis, show a similar size dependence as the quantum chemical results and are in the range of ≈0.6–1.2 eV. Yttrium doping significantly alters the propene adsorption energies for $n = 5$, 12 and 13. Chemical bonding and energy decomposition analysis showed that there is no covalent bond between the cluster and propene, and that charge transfer and other non-covalent interactions are dominant. The natural charges, Wiberg bond indices, and the importance of charge transfer all support an electron donation/back-donation mechanism for the adsorption. Yttrium plays a significant role not only in the propene binding energy, but also in the chemical bonding in the cluster-propene adduct. Propene preferentially binds to yttrium in small clusters ($n < 10$), and to a gold atom at larger sizes. Besides charge transfer, relaxation also plays an important role, illustrating the non-local effect of the yttrium dopant. It is shown that the frontier molecular orbitals of the clusters determine the chemical bonding, in line with the molecular-like electronic structure of metal clusters.

Introduction

Few-atom gold clusters have been shown to be highly active for selected catalytic reactions,[1–3] such as CO oxidation,[4,5] the water-gas shift reaction,[6] O_2 activation,[7] propene epoxidation,[5,8,9] methane activation,[10] and water splitting.[11,12] Gold clusters exhibit high reaction rates, with a strong dependence on the precise cluster size and charge state.[13,14] Small gold clusters were also shown to selectively catalyse propene to propylene oxide,[9] which is an important industrial precursor for a variety of chemicals, such as polyurethane or propylene glycol.

The electronic and geometric properties of gold clusters can be tuned by the introduction of a dopant atom, which also influences the chemical properties of the clusters. For example, the binding energies, as well as the HOMO–LUMO gaps, were found to be enhanced by Mo, Ru, and Co doping.[15] Pd doping also substantially alters the stability patterns of cationic gold clusters.[16] Doping of both neutral and cationic gold clusters with a silver atom reduces their reactivity towards CO,[17,18] while doping neutral gold clusters with vanadium decreases their reactivity towards CO in the size range of 14 to 20 atoms.[19] It was also computationally predicted that the bond between propene and gold clusters can be weakened upon exchanging gold with the less electronegative silver in mixed gold-silver clusters.[20]

The yttrium atom is an interesting dopant to tune the stability and the catalytic activity of the gold clusters. Its size and electronegativity differ significantly from that of a gold atom, and it has unoccupied d orbitals, what makes it a good electron acceptor. It was shown by combined far-infrared multiple photon dissociation spectroscopy and density functional theory computations that yttrium doping also stabilizes the 3D geometries.[21–23] The geometry of pure neutral gold clusters (clusters consisting only of gold atoms are referred to as pure clusters in this paper) is planar up to $n = 10$,[24] while yttrium-doped gold clusters are quasi-planar up to Au_8Y for most cluster sizes. However, Au_4Y has a 3D shape and also $Au_{n-1}Y$ ($n =$ 6–9) clusters are slightly distorted from a perfect planar

[a] Dr. T. Höltzl
Furukawa Electric Institute of Technology
Késmárk utca 28/A, Budapest, 1158 (Hungary)
E-mail: tibor.holtzl@furukawaelectric.com

[b] Dr. J. Vanbuel, Dr. P. Ferrari, Prof. Dr. E. Janssens
Quantum Solid State Physics, KU Leuven
Celestijnenlaan 200d, 3001 Leuven (Belgium)
E-mail: ewald.janssens@kuleuven.be

[c] Dr. T. Höltzl
MTA-BME Computation Driven Chemistry Research Group
Budapest University of Technology and Economics
Szent Gellért tér 4, Budapest, 1111 (Hungary)

[d] J. Barabás, Dr. T. Höltzl
Department of Inorganic and Analytical Chemistry
Budapest University of Technology and Economics
Szent Gellért tér 4, Budapest, 1111 (Hungary)

Supporting information and the ORCID identification number(s) for the author(s) of this article can be found under: https://doi.org/10.1002/chem.201902794.

shape.[23] Electronically, the trivalent yttrium dopant alters the electronic shell structure of the gold clusters, for example, Au_6Y^+ and $Au_{16}Y^+$ both have closed electronic structures with 8 and 18 itinerant electrons, respectively. The enhanced stabilities of these clusters explain their high relative abundance in photofragmentation experiments.[25] Computationally, it was predicted that the CO binding energies of $Au_{n-1}Y$ ($n=2$–10) are lower than that of the corresponding pure clusters.[26]

Gas-phase studies can enhance the understanding of reactions at the molecular level, and allow the investigation of the effect of cluster size, charge and spin state, oxidation number, composition, etc. The bond formation and bond breaking processes are confined to the catalytically active sites, which can be modelled by small clusters.[27] Beside the calculation of the reaction energy, the analysis and the understanding of the chemical interactions between catalyst and reagents is important for rational catalyst design. For cluster-adduct complexes, the changes in bond lengths and charges,[28–30] the frontier orbital and population analysis,[31–33] ionization potentials and electron affinities,[34] and NBO analysis,[35] are commonly used to analyse the chemical bonding.

The donation/back-donation mechanism of ethylene adsorption on gold clusters was inferred from changes in the total charge of the adsorbate and the clusters bond lengths.[28,30] It was shown that CO adsorption on Pd clusters elongates the Pd–Pd and C–O bonds, which supports a donation/back-donation mechanism.[29] In that case, no pronounced correlation was observed between the frontier orbital energies of the clusters and the adsorption energies. On the other hand, it was found that the magnitude of the HOMO–LUMO gap and the charge determine the binding energy of dioxygen to gold clusters.[32–34] It was shown recently that not only the change in the chemical bonding and the electronic structure determines the surface adsorption processes, but also van der Waals interactions can play an important role.[36] In the case of alkoxide adsorption on gold surfaces, these interactions determine the relative stabilities of the intermediates as well as the selectivity of reactions.[37,38]

In the present work we investigate the adsorption of propene on small neutral yttrium-doped gold clusters, $Au_{n-1}Y$ with $n=5$–15, using a combination of gas phase reactivity measurements in a low-pressure collision cell and DFT calculations. This study extends on an earlier experimental study of propene adsorption on pure small neutral gold clusters, Au_n ($n=9$–25) under few-collision conditions.[39] The goal of the present work is to understand the importance of the chemical bonds, charge transfer and non-covalent interactions in the adsorption process and the role of the yttrium dopant atom in this respect. The chemical bonds are analysed in terms of the natural charges, Wiberg indices, Localized Orbital Locator, Bader analysis, as well as by Energy Decomposition Analysis.

Experimental Section

Experimental approach

The applied method for cluster production is described in detail in ref. [40] and is only briefly presented here. The pure and yttrium-doped gold clusters are produced in a dual-target dual-laser vaporization source.[40] Source parameters (carrier gas pressure, laser energies, timing sequence, etc.) are optimized for singly yttrium-doped gold clusters in the size range of 10 to 20 atoms. The clusters are assumed to be thermalized with the source through heat exchange by the He carrier gas.[41] The temperature of the source is controllable in the 100–300 K range by a combination of liquid nitrogen cooling and resistive heating. After expansion into vacuum and passage through a conical skimmer, a molecular beam of clusters is formed. Initially charged particles from the source are electrostatically deflected out of the beam.

The neutral clusters interact with the C_3H_6 molecules in a collision cell that is placed in the flight path of the molecular beam. In order to study the kinetics of the reaction, the pressure of the reactive gas is varied, while the interaction time is fixed by the time that the neutral clusters spend in the reaction cell.[26] Propene gas is introduced continuously by a needle valve. The pressure inside the reaction cell is measured by a capacitance gauge and was varied in the range of 0–0.14 Pa, corresponding to 0–7 collisions per cluster on average. Higher pressures are avoided to prevent signal loss due to deflection of the clusters by collisions with the reaction gas. The neutral clusters and cluster-propene complexes are post-ionized by an F_2 excimer laser (photon energy of 7.89 eV) and extracted into a time-of-flight mass spectrometer ($M/\Delta M=$ 800). The fluence of the ionization laser beam was kept low to minimize photo-induced fragmentation.

In order to extract adsorption energies from the experimentally determined dissociation rates, a statistical approach was applied. The cluster-propene dissociation reaction is a statistical process with a rate depending mainly on the heat capacity of the cluster, its internal temperature and the propene adsorption energy. This statistical analysis was performed using the MassKinetics[42] software package, developed by Drahos et al. and is based on Rice–Ramsperger–Kassel–Marcus (RRKM) theory. A more detailed description of the analysis procedure, as well as examples of its successful application to cluster systems, can be found in ref. [43]. For the energized propene-cluster complexes, the DFT computed frequencies of the ground-state structures were used. For the transition state (TS), we used a "loose" TS model, which is suitable to model simple bond cleavage reactions.[43] For the loose TS, the calculated frequencies of the bare (i.e., cluster without propene) cluster and the propene molecule were used, while the remaining low-frequency bending modes were set to 25 cm^{-1}. Furthermore, adiabatic rotations were taken into account by using a rotational barrier of $E_{RB}=0.1$ eV.

Computational approach

DFT calculations were carried out using the Q-Chem 4.4 and Q-Chem 5.1 quantum chemical software packages.[44] The BP86 generalized gradient functional[45,46] and the LANL2DZ basis set[47–50] were applied to pre-optimize the molecular geometries. Geometries of the most stable Au_n clusters are taken from ref. [51]. For $Au_{n-1}Y$ with $n=5$–10, the geometries were adapted from ref. [21], while larger sizes are obtained from ref. [52]. These structures were assigned by comparison of their IR spectra with experimental data.[21] More accurate single point calculations were carried out on the optimized geometries of the most stable clusters using the TPSSh[53] functional and the DEF2-TZVP[54] basis set in conjunction

with XDM dispersion correction.[55,56] The (75,302) integration grid, as it is implemented in the Q-Chem software, was applied in all cases. The method was tested by reference CCSD(T)/DEF2-TZVPPD calculations[57] for Au_4, Au_6 and Au_5Y clusters using the MRCC program.[58–60] Furthermore, single point CAM-B3LYP/DEF2-TZVP[61] calculations were carried out on the optimized geometries for all sizes.

The initial cluster-propene geometries were systematically generated in π and di-σ bonding modes and subsequently optimized using DFT calculations. In the π-bonded configuration the two carbon atoms coordinate to the same gold atom, while in the di-σ bonding mode they are bound to two neighbouring Au atoms. The barrierless nature of the propene adsorption reaction was confirmed by optimizations starting from initial structures in which the propene molecule was placed 5 Å from the closest atom of the cluster. The interaction between the clusters and the propene is evaluated by the adsorption energy, defined as $E_{ads} = E(Au_{n-1}Y) + E(C_3H_6) - E(Au_{n-1}Y\text{-}C_3H_6)$. The calculated adsorption energy was corrected with the zero-point vibrational energy (defined as $\Delta E_{ZPE} = ZPE_{Au_{n-1}Y} + ZPE_{C_3H_6} - ZPE_{Au_{n-1}Y\text{-}C_3H_6}$). The basis set superposition error (BSSE) was compensated using the counterpoise method.[62,63] The stability of clusters was determined by calculating the total atomization energy, defined as $E_{ta} = -[E(Au_n) - n \cdot E(Au)]/\ n$ for the gold clusters and as $E_{ta} = -[E(Au_{n-1}Y) - (n-1) \cdot E(Au) - E(Y)]/\ n$ for the yttrium-doped clusters. With this convention larger positive values indicate a larger energetic stabilization.

Energy decomposition and charge transfer analysis,[64] as implemented in Q-Chem 5.1, was carried out to analyse the nature of the cluster-propene interaction and to determine the orbital interaction in the complexes. The calculated intermolecular binding energy contains Coulomb electrostatic, Pauli repulsion, dispersion, polarization and charge-transfer terms. The orbital-orbital interactions were investigated using the ALMO-EDA method and Complementary Occupied-Virtual Pairs (COVPs).[64] Each COVP consists of an occupied orbital of one part of the complex (electron donor) and a virtual of the other (electron acceptor). The chemical bonding was analysed in terms of the Localized-Orbital Locator (LOL), computed using the D-Grid[65–67] code, Bader[68] theory and NBO analysis, involving Wiberg bond indices and natural charges[69,70] calculations computed with the NBO 6 program suite integrated into the Q-Chem 4.4. software package.

Molecules were visualized using the PyMol program.[71] Kohn–Sham orbitals were visualized using IQmol,[72] while the Molden program was used for plotting the COVP orbitals.[73,74] The Multiwfn program was applied for Bader analysis.[75]

Results and Discussion

A. Mass spectrometric results

Mass spectra for gold-yttrium clusters interacting with C_3H_6 have been recorded for a range of reaction gas pressures. A part of a representative mass spectrum is shown in Figure 1, in which one can distinguish pure Au_n clusters, doped $Au_{n-1}Y$ clusters, and the corresponding cluster-propene complexes, Au_n-C_3H_6 and $Au_{n-1}Y$-C_3H_6. For the smallest clusters, $n < 9$ (not shown in Figure 1), the intensity ratio of the complexes to the corresponding bare clusters, $I_{AuY\text{-}C_3H_6}/I_{AuY}$ is low (< 5%). This is a consequence of the small heat capacity of these clusters, which cannot accommodate the heat of formation of the cluster-propene complexes, thus dissociating faster than the time scale of the experiment.[16,19,39] The small signals in the mass spectrum in between the bare metal clusters and the cluster-propene complexes correspond to water and oxygen contaminations.

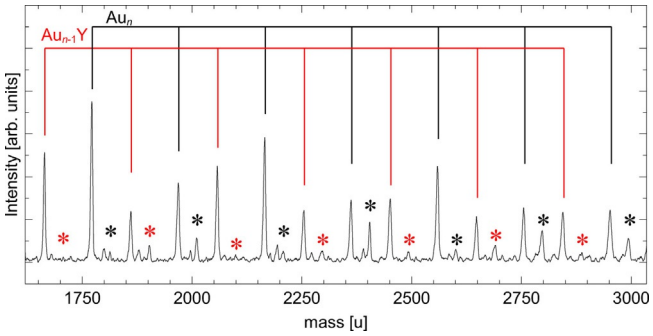

Figure 1. Mass spectrum of Au_n and $Au_{n-1}Y$ ($n = 9$–15) clusters that have reacted in the collision cell with C_3H_6 molecules ($T = 110$ K, $p_{C_3H_6} = 0.04$ Pa). Pure Au_n clusters are indicated by black lines. Red lines point to the $Au_{n-1}Y$. Black and red asterisks indicate Au_n-C_3H_6 and $Au_{n-1}Y$-C_3H_6 complexes, respectively. Other small signals are water and oxygen contaminations.

An example of the pressure-dependent cluster-propene complex intensity is shown in Figure 2. Intensities of the complexes are normalized by the intensities corresponding to clusters before reaction, $I_{rel} = I_{AuY\text{-}C_3H_6}/(I_{AuY} + I_{AuY\text{-}C_3H_6})$. This example illustrates how substitution of a gold atom by an yttrium atom in the neutral Au_{12} cluster reduces the probability of cluster-propene complex formation.

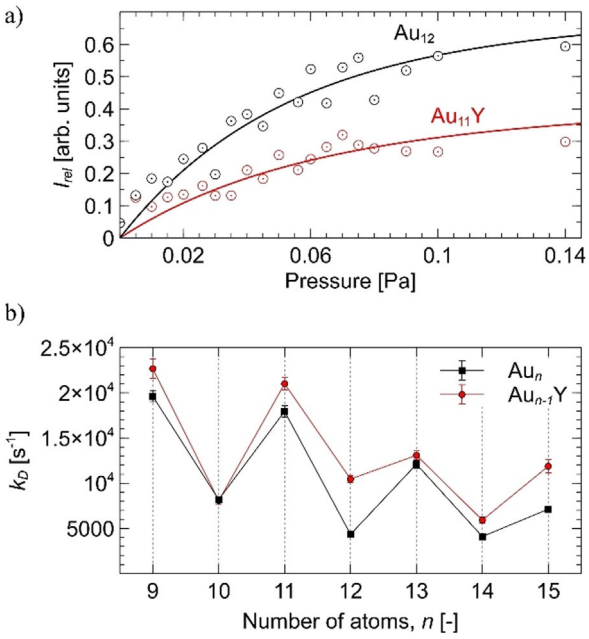

Figure 2. a) Relative intensities of Au_{12}-C_3H_6 (black) and $Au_{11}Y$-C_3H_6 (red) as function of the pressure in the collision cell. The solid black and red lines are fits using the rate law determined from the reaction mechanism with k_D as only fitting parameter and using the hard sphere collision rate for k_F. b) Experimentally determined dissociation rate coefficients k_D of Au_n-C_3H_6 and $Au_{n-1}Y$-C_3H_6 ($n = 9$–15) at 110 K. The error bars were calculated as the fitting errors with 95% confidence interval, assuming a hard-sphere collision rate for the forward rate.

In line with earlier experiments, the interaction between a cluster and a small molecule in a low-pressure reaction cell can be described by a two-stage reaction mechanism.[39,76] Inside the reaction cell both the adsorption of a propene molecule, leading to the formation of propene-cluster complex with bimolecular association rate coefficient k_F, and the dissociation of this complex to propene and cluster, with unimolecular dissociation rate coefficient k_D, take place [Eq. (1)]:

$$Au_{n-1}M + C_3H_6 \xrightarrow{k_F} Au_{n-1}M - C_3H_6 \xrightarrow{k_D} Au_{n-1}M + C_3H_6 \quad (1)$$

(where M = Au or Y)

Because of the absence of a buffer gas in the reaction cell, unimolecular dissociation is the main channel to cool the complexes. Outside the reaction cell, only dissociation of the complex can occur. Earlier work on pure gold[39] and vanadium-doped gold[19] clusters interacting with C_3H_6 and CO, respectively, demonstrated that the formation rate coefficient for these reactions can be approximated by the hard sphere collision rate, $k_F = \sigma v$, with σ the collisional cross-section and v the relative velocity between the cluster and the molecule. A hard sphere collision cross section implies that each collision leads to the formation of a complex and that there is no activation barrier or steric factor involved.

By fitting the solution of the rate law determined on basis of Equation (1) to the experimentally recorded pressure dependent intensities (see ref. [19] for details), the dissociation rates of the clusters-propene complexes, k_D, are obtained for $n = 9$–15. These rates are plotted in Figure 2 b. For smaller sizes the intensities of the cluster-propene complexes were too low to allow reliable fits, since k_D^{-1} is much shorter than the timescale of the experiment.

For pure gold clusters, the size dependence has already been discussed in ref. [39]. The yttrium doping increases the dissociation rate in the $n = 9$–15 size range, except for $n = 10$ and 13, where the dissociation rates of Au_n-C_3H_6 and Au_{n-1}Y-C_3H_6 are nearly equal. k_D shows a clear odd-even alternation both for the pure and yttrium-doped gold clusters; clusters with an even number of atoms have a lower cluster-propene dissociation reaction rate.

B. Computed lowest energy structures of Au_n-C_3H_6 and Au_{n-1}Y-C_3H_6

The energetically most favourable structures of Au_n and Au_{n-1}Y ($n = 5$–15) and the corresponding cluster-propene complexes are shown in Figure 3.

It is well known that neutral Au_n clusters are planar up to surprisingly large sizes. The energy differences between the most stable 2D and the 3D isomers are small in the range of $n = 10$–13, so the different computational methods may lead to a different transition size.[24,51,77–79] According to our computations, the 2D structure of Au_{10} is more stable than the 3D one, while for Au_{11} the three-dimensional structure is the energetically lowest lying isomer, in agreement with refs. [24, 77–79]. The yttrium-doped Au_{n-1}Y clusters prefer two-dimensional structures only up to Au_8Y.[21] This lower 2D to 3D transition

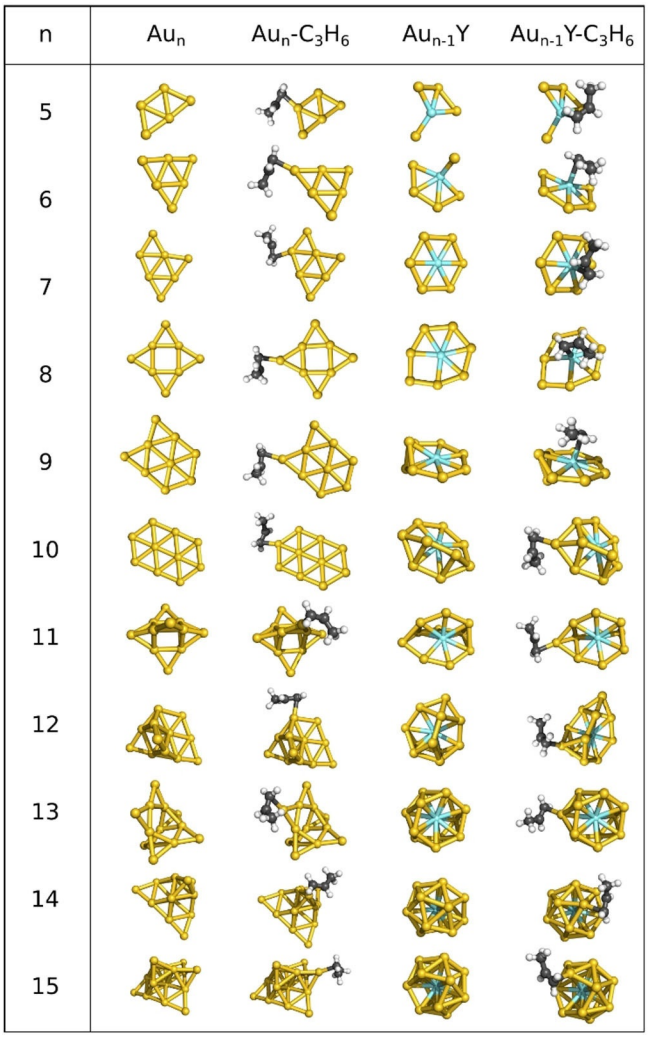

Figure 3. Optimized structures of the lowest energy Au_n and Au_{n-1} ($n = 5$–15) clusters and the corresponding Au_n-C_3H_6 and Au_{n-1}Y-C_3H_6 complexes, calculated using the BP86/LANL2DZ method. Au, yellow; Y, blue; C, grey; H, white.

size is explained by the involvement of the yttrium d electrons in the bonding of the doped clusters.[21] Larger Au_{n-1}Y clusters have basket-like structures ($n = 11$–13) or even complete cages for $n > 14$.

For the pure gold clusters, propene binds preferentially on-top of a low-coordinated gold atom through its C=C double bond, which corresponds to a π-bonding mode. This is similar to the ethylene adsorption on neutral gold clusters.[28] In the case of the Au_{n-1}Y clusters, propene binds to the yttrium for $n < 10$, while for larger clusters the propene connects to a gold atom. This adsorption site preference correlates with the structural size evolution of the clusters: propene prefers to bind to yttrium for clusters that have (quasi) 2D structures but binds to a gold atom in clusters with a 3D structure, where the yttrium atom is less accessible. As Au_8Y is in the 2D to 3D transition region, propene binding to yttrium is preferred by only 0.04 eV over binding to gold. In line with the binding rules proposed by Chrétien et al.,[80] propene generally prefers to bind to a low-coordinated atom, where one of the low-lying unoccupied

orbitals of the bare cluster has a large lobe (see Figures S1 and S2 in the Supporting Information).

C. Propene adsorption energies

Propene adsorption energies are obtained by modelling the experimentally measured dissociation rates with Rice–Ramsperger–Kassel–Marcus (RRKM) theory (Figure 4). Due to the barrierless propene adsorption, we apply the loose transition state model, where entropic considerations are of importance. Figure 4 illustrates the propene adsorption energies for the pure and doped gold clusters modelled using RRKM and calculated using DFT. The absolute propene binding energies obtained by the RRKM model are systematically larger than the DFT calculated values by about 0.1–0.2 eV. The maximum differences between the CAM-B3LYP/DEF2-TZVP and the TPSSh-XDM/DEF2-TZVP binding energies are 0.06 eV for Au_n and 0.11 eV for the $Au_{n-1}Y$ ($n=5$–15) clusters, while the average unsigned differences are $\approx$0.03 and $\approx$0.06 eV, respectively. Thus the two different functionals yield approximately the same result (Figure S3 in the Supporting Information). The TPSSh-XDM/DEF2-TZVP results deviate from the CCSD(T)/DEF2-TZVPPD by -0.24 to -0.30 eV (Table S1 in the Supporting Information). This shows that the DFT accurately describes the size-to-size variation of the binding energies, while the absolute values are underestimated compared to the benchmark.

The size-dependent variation and the effect of yttrium doping on the adsorption energies show similar patterns in Figures 4a and b. Yttrium doping has a remarkable effect on the propene adsorption energy at cluster sizes $n=5$–7 and 13–14. In the case of $n=13$, both the DFT and the RRKM computation show that the propene adduct of the yttrium-doped cluster is less stable than that of the pure gold cluster, while the opposite effect is observed in the case of $n=14$. In both sizes the propene molecule connects to a gold atom, which implies an indirect effect of the yttrium dopant. Other interesting sizes are Au_4Y and Au_6Y where yttrium doping lowers the adsorption energy, while the opposite effect is observed in the case of Au_5Y; although in the three doped clusters propene binds to the yttrium atom. In the case of the other sizes, the effect of the yttrium doping is smaller. For $n=11$, yttrium doping stabilizes the complex, while for $n=12$ the doping has a destabilization effect. For $n=9$ and 15, RRKM predicts nearly equal adsorption energies for the doped and pure clusters, while somewhat lower adsorption energies for the doped clusters were found by the DFT calculations. Similar small differences, in the order of the accuracy of the methods, were also observed for $n=10$.

The adsorption energies of smaller clusters ($n=5$–8) could only be computed using DFT calculations, since propene complexes were not observed in this size range (see Experimental Section for the reason). The adsorption energy of the propene molecule to $Au_{n-1}Y$ shows little size dependence ($E_{ads}=$ $\approx$0.8 eV) in this size range, while for the pure gold clusters the adsorption energy has a pronounced minimum at Au_6. Interestingly, although the propene molecule prefers to bind to the yttrium dopant atom, the doping itself lowers the adsorption energy for the small ($n=5$–9) cluster sizes, except for $n=6$.

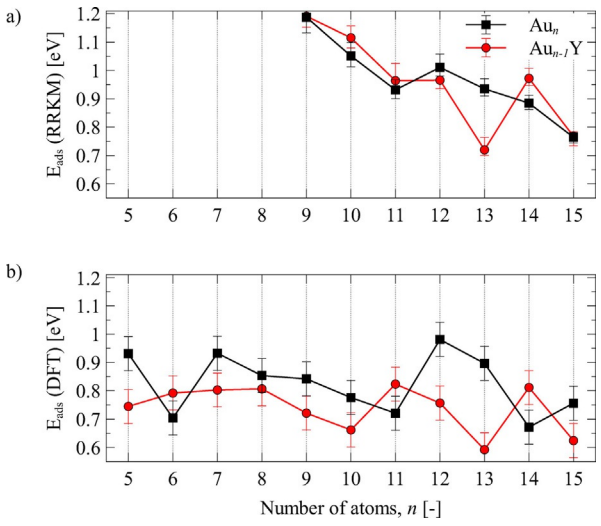

Figure 4. Adsorption energies of C_3H_6 on Au_n and $Au_{n-1}Y$ (a) for $n=9$–15 as derived from the experiments by employing the RRKM model with loose transition state, and (b) for $n=5$–15 using the total energies of the DFT computed lowest energy structures. Error bars on the RRKM modelled values have been estimated by scaling all vibration frequencies by a factor 0.9 and a factor 1.1. The uncertainty on the frequencies dominated the uncertainty on the experimentally measured k_d values. The error bars do not account for possible systematic uncertainties on the underlying assumptions of the RRKM model. Error bars of the DFT computations were estimated using CCSD(T)/DEF2-TZVPPD benchmarks of propene adsorption on Au_4, Au_6 and Au_5Y (Figure S3 and Table S1 in the Supporting Information).

D. Chemical bonding analysis

Localized orbital locators (LOL) and bond critical points of the electron density: LOL is a three-dimensional function of the kinetic energy density (τ) and its interpretation is based on the fact that τ is small in the bonding region.[65–67] LOL correctly shows the shell structure of the atoms and the different elements of the chemical bonding (bonds, lone pairs etc.), even if there is strong delocalization in the molecule. The LOL profiles of Au_9, Au_6Y and $Au_{10}Y$ and their propene adducts are shown in Figure 5, while the corresponding LOL profiles for other Au_n and $Au_{n-1}Y$ ($n=5$–15) sizes are available in Figures S4–S7 of the Supporting Information. LOL profiles of pure gold clusters indicate the formation of two-electron three-centre bonds between the gold atoms. Similar bonds are not formed in the case of small $Au_{n-1}Y$ clusters, as no LOL localization domain is observed between yttrium and gold. The LOL profiles of the cluster-propene complexes do not exhibit a basin between the clusters and propene, thus there is no covalent bond between these moieties. The LOL of the adducts is approximately the combination of that of the reactants, except for the slightly increased localization near to the propene adsorption site. The topological analysis of the electron density (Bader analysis) defines the chemical bonds by a Bond Critical Point (BCP) and the corresponding bond paths (gradient paths) leading to the nuclei. A covalent bond is characterized by a $\approx 10^{-1}$ a.u. electron density at the bond critical point (BCP) and a negative

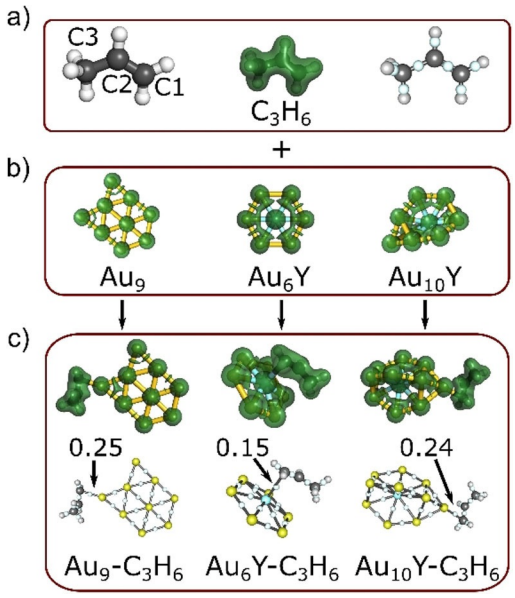

Figure 5. Localized Orbital Locator isosurfaces (green lobes) of (a) C_3H_6, (b) Au_9, Au_6Y and $Au_{10}Y$ clusters, and (c) Au_9-C_3H_6, Au_6Y-C_3H_6 and $Au_{10}Y$-C_3H_6 complexes (LOL = 0.3). In (c) the values of the M-C1 Wiberg bond indices are also given. Bond Critical Points are marked with light blue dots. (M = Au or Y).

Laplacian, while electrostatic interactions and ionic bonds are characterized by a lower electron density at the BCP ($\approx 10^{-2}$ a.u.), and a positive Laplacian.[81] The electron density at the BCP in the Au_n-C_3H_6 complexes is low (about 0.06–0.08). In the $Au_{n-1}Y$-C_3H_6 complexes, the value depends on the propene binding site. If propene is bound to the exposed Y dopant ($n = 5$–9), the electron density at the BCP between propene and the cluster is about 0.03 a.u., while for complexes having Au-C interactions ($n = 10$–15) it is between 0.07–0.08 a.u. The Laplacian of the electron density has a small positive value in the BCP—around 0.06 and 0.15 a.u. for propene binding to yttrium and gold, respectively (see values in Table S2 of the Supporting Information). These values are indicative for electrostatic interactions between the adducts, which is in line with the results from the LOL analysis.

Natural charges and bond indices: For the bare gold clusters, we found small charge separation (Table S3 in the Supporting Information). However, in $Au_{n-1}Y$ clusters, gold atoms donate electrons to the yttrium d atomic orbitals (Figure S8 in the Supporting Information). In the cluster-propene complexes no charge separation was observed between the cluster and the propene molecule (Figure S10). The Wiberg bond index between two atoms A-B is the sum of the corresponding squared elements of the density matrix. For typical chemical bonds, its value is close to the formal bond order. Here, the bond indices between each carbon atom of propene and the metal atom M (M = Au or Y) of the cluster to which the propene attaches are also low, about 0.25 if M = Au and about 0.15 if M = Y (Table 1). Upon propene adsorption to a gold atom of the cluster, the C1 and C2 atoms become more negatively charged (see Table 1 and Figure S11 in the Supporting Information). This, along with the decreasing C1–C2 Wiberg bond indices implies a donation/back-donation mechanism for propene adsorption.[80] The interaction is slightly different if propene binds to the Y dopant. In this case, the natural charge of the C1 atom becomes even more negative, while the C2 atom is less negatively charged compared to the isolated propene molecule. The decrease of C1–C2 Wiberg bond index is smaller if propene binds to yttrium compared to the case of gold. This suggests that the extent of the donation/back-donation is smaller if propene attaches to the yttrium dopant atom as compared to a gold atom.

Table 1. Natural charges of carbon atoms in propene and Wiberg bond indices between the carbon atoms in propene (C1–C2, C2–C3) and between the carbon atoms and the metal atom M of the clusters to which propene attaches (M–C1, M–C2 with M = Au or Y) (See Figure 5 for labelling of the carbon atoms).

	C_3H_6	Au_9-C_3H_6	$Au_{10}Y$-C_3H_6	Au_6Y-C_3H_6
Natural charge				
C1	−0.39	−0.50	−0.50	−0.55
C2	−0.17	−0.19	−0.20	−0.08
C3	−0.61	−0.63	−0.63	−0.64
Wiberg bond index				
C1-C2	1.98	1.67	1.68	1.87
C2-C3	1.06	1.07	1.07	1.07
M-C1	–	0.24	0.23	0.14
M-C2	–	0.21	0.20	0.07

Energy decomposition analysis: The analysis of the LOL, the electron density as well as the natural charges and the Wiberg bond indices all support that there is no covalent bond between the clusters and propene, and the cluster-propene interaction results from charge transfer and other non-covalent interactions. The character of this non-covalent bonding is further investigated using energy decomposition analysis (EDA).[64] This approach decomposes the interaction energy into different interactions and quantifies their importance. We decompose the adsorption energy in the following form [Eq. (2)]:

$$E_{\text{adsorption}} = E_{\text{charge transfer}} - E_{\text{frozen}} + E_{\text{polarization}} - E_{\text{relaxation}} + E_{\text{dispersion}} + \Delta E_{\text{ZPE}} \quad (2)$$

In Equation (2), the dispersion term is computed using the XDM dispersion correction. The relaxation term accounts for the energy penalty to distort the cluster and propene geometry during the adsorption process. The frozen term is due to the permanent electrostatic interactions and Pauli repulsion. The permanent electrostatic interaction is expected to be small since both fragments are neutral and there is no strong charge separation in either the cluster or the propene molecule. The polarization term is defined as the energy lowering due to the intra-fragment relaxation of the frozen molecular orbitals, that is, internal charge re-organization in the cluster and propene during the reaction. The charge transfer energy term is defined as the energy lowering due to the electron transfer from an occupied orbital of one fragment to the unoccupied orbital of

the other. It essentially describes the presence of electron donation/back-donation in the cluster-propene complex.

In pure clusters, the frozen (negative contribution) and the charge transfer (positive contribution) terms have the highest contributions to the total energy and both contributions show similar tendencies (Figure 6). The frozen term is repulsive, but the charge transfer term overcompensates this energy penalty. This is also true for the $Au_{n-1}Y$ clusters, although the magnitudes of both terms are much larger if propene binds to an Au atom ($\approx$1.5–2.5 eV for $Au_{n-1}Y$ with $n \geq 10$) compared to the Y dopant ($\approx$0.2–0.6 eV for $Au_{n-1}Y$ with $n < 10$). This binding site dependency can be explained by the smaller Pauli repulsion in the case of attachment to the yttrium dopant (yttrium has only one d electron) and also to the larger charge transfer in the case of an Au binding site (Au is more electronegative than Y).

The polarization term follows a similar trend in the pure and doped clusters if $n \geq 10$, where propene binds to gold, while for $n < 10$ the polarization effect is smaller in $Au_{n-1}Y$ than in Au_n. This is in line with the importance of the electronegativity of the dopant atoms. It must also be noted that the charge transfer, frozen, and polarization terms are nearly constant for $Au_{n-1}Y$ $n < 10$, which explains the limited size dependence of the propene adsorption energy in this size range.

It is well visible in Figure 6 that the total propene binding energy on pure gold clusters is determined mainly by the sum of the frozen, the polarization and the charge transfer terms (see Figure S12 for details in the Supporting Information), while the relaxation, the dispersion and the zero-point energy

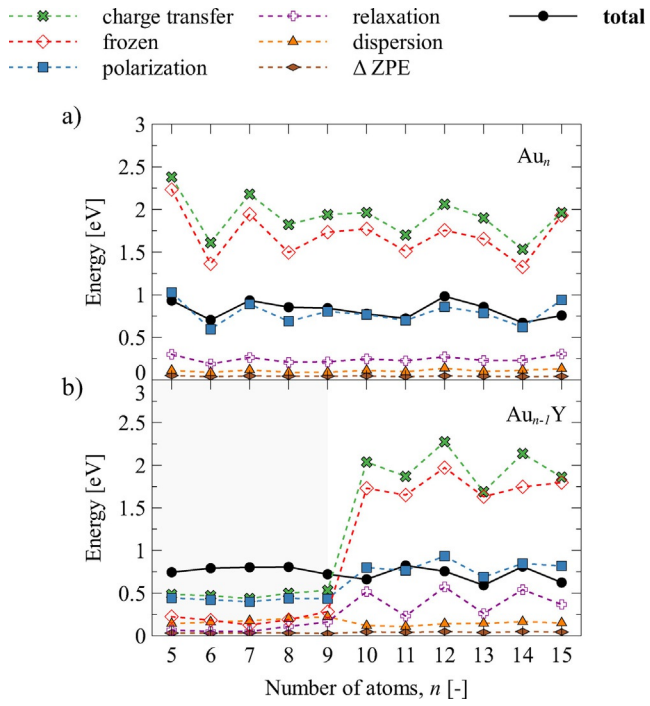

Figure 6. Energy decomposition analysis of the propene adsorption energy (total) for a) Au_n and b) $Au_{n-1}Y$ ($n = 5$–15) clusters. Grey background shows the complexes where propene is attached to the Y dopant. Full and hollow symbols are used for positive and negative contributions to the adsorption energy, respectively.

have only smaller, and weakly size-dependent contributions. Interestingly, while in organic molecules the dispersion interaction generally increases with their size, in the case of cluster-propene adducts we found that it only shows a small size dependence without a clear tendency and is in the range of 0.08 to 0.22 eV.

The charge-transfer term correlates with the total adsorption energy (see Figure S13 in the Supporting Information), showing that the binding is determined mainly by the charge transfer between propene and the cluster, in agreement with ref. [80]. The variation of the charge transfer term with the cluster size explains for instance that the binding energy of propene to Au_6 is lower, while that of the Au_{12} is higher than for their neighbours.

On the other hand, in yttrium-doped gold clusters also the relaxation has an important effect. Relaxation is not only larger than in the pure gold clusters, but also shows a strong size dependence. This is in line with the observation that the propene binding energy of yttrium-doped gold clusters has a more complex size dependence compared to the pure gold clusters. In addition, due to the large relaxation, there is no correlation between the charge transfer term and the total binding energy of propene. However, by subtracting the relaxation term from the total binding energy a good correlation can be observed (see Figure S14 and S15 in the Supporting Information). Charge transfer has a small size dependence when propene attaches to the yttrium atom, which nicely correlates with the observed propene binding energy. On the other hand, if propene binds to a gold atom, the larger charge transfer generally results in a stronger binding. This clearly shows the important role of charge transfer in the propene binding to yttrium-doped gold clusters. Overall, in pure gold clusters the charge transfer, the polarization and the frozen terms determine the size dependent stability, while in yttrium-doped gold clusters the relaxation is also important.

In the case of $n = 12$ the large difference between the calculated propene adsorption energies (Figure 4) on the pure and doped gold clusters can be explained with the magnitudes of the relaxation terms. In the $n = 13$ case, however, the relaxation terms have similar values and hence the smaller frozen term leads to the enhanced stability of Au_{13}-C_3H_6 compared to $Au_{12}Y$-C_3H_6. For $n = 14$ the sum of the polarization, charge transfer and frozen terms is much smaller in the pure cluster and the larger relaxation term of $Au_{13}Y$-C_3H_6 does not compensate for it. Therefore, at this size the yttrium-doped cluster-propene complex is more stable.

Orbital interactions: In the molecular orbital framework, the charge transfer is represented by the electron donation from an occupied orbital of one of the reagents to a virtual orbital of the other reagent. The computed complementary occupied/virtual pairs (COVPs) demonstrate that in each cluster-propene adduct only a few orbital interactions dominate the charge transfer. Figure 7 shows the main occupied-virtual pairs for selected cluster sizes. In the case of pure gold clusters, there are two main complementary occupied-virtual orbital pairs in which donation/back-donation occurs. In one pair, the π orbital of propene donates electrons to the gold s orbitals. In the

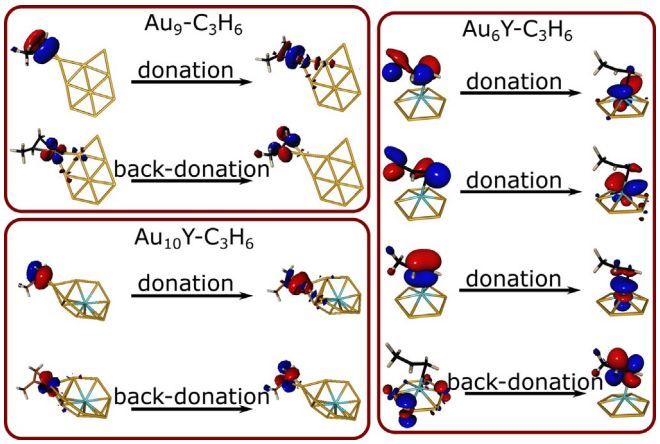

Figure 7. Occupied virtual orbital pairs of the selected Au_9-C_3H_6, Au_6Y-C_3H_6 and $Au_{10}Y$-C_3H_6 complexes.

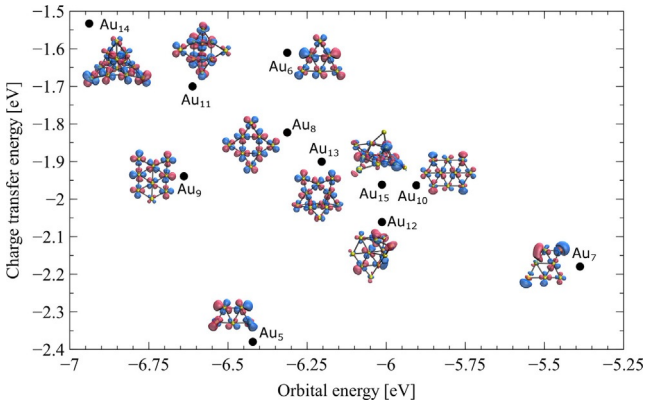

Figure 8. Correlation between the orbital energies of orbitals close to the HOMO/SOMO of the bare clusters, participating in charge transfer bonds, and the charge transfer energies in the cluster-propene complex.

other COVP pair, the direction is opposite: gold donates d electrons to the π^*-orbital of propene. In line with bi-directional donation/back-donation, the charge transfer energy is large, but there is only a small charge separation, as quantified by the natural charges (Figure S10 in the Supporting Information). The size dependence of the charge transfer term is slightly more complicated in the case of yttrium-doped clusters, where donation seems to be the main factor up to $n=9$, resulting in an increased charge separation (see Figure S10 in the Supporting Information). For the larger $Au_{n-1}Y$ ($n \geq 10$) clusters, the situation is similar to the pure gold clusters. The donation mainly occurs from propene π-orbital to the s and p atomic orbitals of gold and the d atomic orbitals of yttrium. The back-donation is primarily from the d orbitals of Y and the s, p and d atomic orbitals of Au to the propene π^*-orbital.

The local nature of the charge transfer bond is well visible in Figure 7. It turns out that gold donates electrons from its d atomic orbital whose symmetry matches that of the propene π^* bond. Thus, only d atomic orbitals with the proper symmetry can participate in the charge transfer bond. We expect that an occupied molecular orbital close to the HOMO or SOMO (semi occupied molecular orbital, for systems with an unpaired electron), having a high contribution from the metal d atomic orbitals, determine the charge transfer from the cluster to propene. Figure 8 indeed shows that for Au_n the trend of the energies of these orbitals is similar to that of the charge transfer. This relates the molecular orbitals of the bare cluster to the propene binding. However, the relationship is not perfect (especially for Au_5, but to a lesser extend for Au_6 and Au_9) as not only the orbital energies, but for example, also the overlaps, are important for the interaction strength.

The propene binding to yttrium-doped gold clusters is more complicated. As discussed earlier in this paper, the relaxation term shows a large size dependence, thus the geometric distortion of the reactants during the cluster-propene adduct formation is large. Therefore, the orbital energies of the clusters change considerably during the propene adsorption and we did not observe any correlation between the orbital and charge transfer energies.

Conclusions

In summary, we studied the effect of yttrium doping on the reactivity of small Au_n clusters with propene by joint gas phase reactivity measurements in a low-pressure collision cell and DFT computations.

The experimental cluster-propene complex dissociation rates are dopant and size dependent and are generally larger for the $Au_{n-1}Y$ clusters, especially for sizes $n>13$. Adsorption energies on pure and yttrium-doped gold clusters are estimated from RRKM analysis and compared to those predicted by DFT. The two different methods give similar tendency for adsorption energies: yttrium doping generally lowers the adsorption energy, except for $n=6$, 11 and 14. The lowering is particularly strong for $n=5$, 7, 12 and 13.

The small population of the yttrium d atomic orbitals for $n<10$, makes it the favoured propene adsorption site, but for larger ($n\geq10$) clusters the yttrium d electron population is increased, and propene connects to a gold atom. The preferred location for propene adsorption is explained by the analysis of the low-lying unoccupied molecular orbital of the corresponding bare clusters, which is in line with the observed donation/back-donation mechanism. The analysis of the chemical bonding showed that there is no covalent bond between the clusters and propene, and that the charge transfer and other non-covalent interactions are responsible for the attractive interaction.

The energy decomposition analysis showed that the charge transfer is the most important term for the propene binding, while in the case of yttrium-doped gold clusters the relaxation is also significant. The charge-transfer bonding is local and only the metal d atomic orbital that matches the propene π^* symmetry participates in the charge donation from the cluster to the propene. On the other hand, propene donates electrons to the unoccupied valence s metal orbital. Therefore, the preferred binding site can be predicted by the analysis of the high-lying occupied and low-lying unoccupied molecular orbitals and by identifying the metal atoms where these atomic orbitals have large lobe. In addition, in the case of pure gold clusters the trend of the corresponding molecular orbitals is

similar to the charge-transfer energy. This relates the bare cluster's molecular orbital energies to the propene binding. Thus, in contrary to the metal surfaces, not the d band centre, but the frontier orbital energies determine the chemical bonding in these clusters.

Thus, we showed in this paper that the non-covalent interactions and the charge transfer are responsible for the propene binding on pure and yttrium-doped gold clusters. The adsorption energy of propene on gold clusters and the non-covalent interactions between the cluster and propene can be tuned by yttrium doping, which opens the way towards rational design of cluster catalysts.

Acknowledgements

This work is supported by the KU Leuven–Budapest University of Technology and Economics joint research funding (CELSA/18/032). The authors thank Prof. Tamás Veszprémi for the fruitful discussions and for his valuable comments. The authors also thank Prof. Mihály Kállay for providing us the MRCC program. P.F. and J.V. acknowledge the FWO (Research Foundation Flanders) for a postdoctoral grant and a PhD fellowship, respectively.

Conflict of interest

The authors declare no conflict of interest.

Keywords: adsorption · clusters · gas phase · gold · reaction

[1] Z. Luo, A. W. Castleman Jr., S. N. Khanna, *Chem. Rev.* **2016**, *116*, 14456 – 14492.
[2] S. J. Freakley, Q. He, C. J. Kiely, G. J. Hutchings, *Catal. Lett.* **2015**, *145*, 71 – 79.
[3] M. Haruta, *Catal. Today* **1997**, *36*, 153 – 166.
[4] M. Okumura, M. Haruta, *Catal. Today* **2016**, *259*, 81 – 86.
[5] T. V. Choudhary, D. W. Goodman, *Top. Catal.* **2002**, *21*, 25 – 34.
[6] X. Zhang, J. Xue, Y. Meng, M. Qian, S. Xia, Z. Ni, *J. Fuel Chem. Technol.* **2017**, *45*, 1473 – 1480.
[7] R. Pal, L.-M. Wang, Y. Pei, L.-S. Wang, X. C. Zeng, *J. Am. Chem. Soc.* **2012**, *134*, 9438 – 9445.
[8] T. Hayashi, K. Tanaka, M. Haruta, *J. Catal.* **1998**, *178*, 566 – 575.
[9] S. Lee, L. M. Molina, M. J. López, J. A. Alonso, B. Hammer, B. Lee, S. Seifert, R. E. Winans, J. W. Elam, M. J. Pellin, S. Vajda, *Angew. Chem. Int. Ed.* **2009**, *48*, 1467 – 1471; *Angew. Chem.* **2009**, *121*, 1495 – 1499.
[10] S. M. Lang, T. M. Bernhardt, V. Chernyy, J. M. Bakker, R. N. Barnett, U. Landman, *Angew. Chem. Int. Ed.* **2017**, *56*, 13406 – 13410; *Angew. Chem.* **2017**, *129*, 13591 – 13595.
[11] Z. Ding, L. Yan, Z. Li, W. Ma, G. Lu, S. Meng, *Phys. Rev. Materials* **2017**, *1*, 045404.
[12] S. Zhao, R. Jin, H. Abroshan, C. Zeng, H. Zhang, S. D. House, E. Gottlieb, H. J. Kim, J. C. Yang, R. Jin, *J. Am. Chem. Soc.* **2017**, *139*, 1077 – 1080.
[13] M. Schlangen, H. Schwarz, *Catal. Lett.* **2012**, *142*, 1265 – 1278.
[14] A. W. Castleman, Jr., *Catal. Lett.* **2011**, *141*, 1243 – 1253.
[15] D. Hossain, C. U. Pittman, Jr., S. R. Gwaltney, *J. Inorg. Organomet. Polym. Mater.* **2014**, *24*, 241 – 249.
[16] P. Ferrari, H. A. Hussein, C. J. Heard, J. Vanbuel, R. L. Johnston, P. Lievens, E. Janssens, *Phys. Rev. A* **2018**, *97*, 052508.
[17] J. De Haeck, N. Veldeman, P. Claes, E. Janssens, M. Andersson, P. Lievens, *J. Phys. Chem. A* **2011**, *115*, 2103 – 2109.
[18] M. Neumaier, F. Weigend, O. Hampe, M. M. Kappes, *Faraday Discuss.* **2008**, *138*, 393 – 406.
[19] H. T. Le, S. M. Lang, J. D. Haeck, P. Lievens, E. Janssens, *Phys. Chem. Chem. Phys.* **2012**, *14*, 9350 – 9358.
[20] S. Chrétien, M. S. Gordon, H. Metiu, *J. Chem. Phys.* **2004**, *121*, 9931 – 9937.
[21] L. Lin, P. Claes, P. Gruene, G. Meijer, A. Fielicke, M. T. Nguyen, P. Lievens, *ChemPhysChem* **2010**, *11*, 1932 – 1943.
[22] L. Lin, P. Claes, T. Höltzl, E. Janssens, T. Wende, R. Bergmann, G. Santambrogio, G. Meijer, K. R. Asmis, M. T. Nguyen, P. Lievens, *Phys. Chem. Chem. Phys.* **2010**, *12*, 13907 – 13913.
[23] L. Lin, T. Höltzl, P. Gruene, P. Claes, G. Meijer, A. Fielicke, P. Lievens, M. T. Nguyen, *ChemPhysChem* **2008**, *9*, 2471 – 2474.
[24] D. A. Götz, R. Schäfer, P. Schwerdtfeger, *J. Comput. Chem.* **2013**, *34*, 1975 – 1981.
[25] W. Bouwen, F. Vanhoutte, F. Despa, S. Bouckaert, S. Neukermans, L. T. Kuhn, H. Weidele, P. Lievens, R. E. Silverans, *Chem. Phys. Lett.* **1999**, *314*, 227 – 233.
[26] L. Lin, P. Lievens, M. T. Nguyen, *Chem. Phys. Lett.* **2010**, *498*, 296 – 301.
[27] H. Schwarz, *Angew. Chem. Int. Ed.* **2015**, *54*, 10090 – 10100; *Angew. Chem.* **2015**, *127*, 10228 – 10239.
[28] A. Lyalin, T. Taketsugu, *J. Phys. Chem. C* **2010**, *114*, 2484 – 2493.
[29] B. Kalita, R. C. Deka, *Eur. Phys. J. D* **2009**, *53*, 51 – 58.
[30] S. M. Lang, T. M. Bernhardt, J. M. Bakker, B. Yoon, U. Landman, *J. Phys. Condens. Matter* **2018**, *30*, 504001.
[31] D. R. Kauffman, D. Alfonso, C. Matranga, H. Qian, R. Jin, *J. Am. Chem. Soc.* **2012**, *134*, 10237 – 10243.
[32] O. Lopez-Acevedo, K. A. Kacprzak, J. Akola, H. Häkkinen, *Nat. Chem.* **2010**, *2*, 329 – 334.
[33] H. X. Shi, W. G. Sun, X. Y. Kuang, C. Lu, X. X. Xia, B. L. Chen, A. Hermann, *J. Phys. Chem. C* **2017**, *121*, 24886 – 24893.
[34] M. Okumura, Y. Kitagawa, M. Haruta, K. Yamaguchi, *Chem. Phys. Lett.* **2001**, *346*, 163 – 168.
[35] A. Prestianni, A. Martorana, F. Labat, I. Ciofini, C. Adamo, *J. Phys. Chem. B* **2006**, *110*, 12240 – 12248.
[36] F. Cheenicode Kabeer, W. Chen, R. J. Madix, C. M. Friend, A. Tkatchenko, *J. Phys. Chem. C* **2017**, *121*, 27905 – 27914.
[37] J. C. F. Rodriguez-Reyes, C. G. F. Siler, W. Liu, A. Tkatchenko, C. M. Friend, R. J. Madix, *J. Am. Chem. Soc.* **2014**, *136*, 13333 – 13340.
[38] C. G. Siler, R. J. Madix, C. M. Friend, *Faraday Discuss.* **2016**, *188*, 355 – 368.
[39] E. Janssens, H. T. Le, P. Lievens, *Chem. Eur. J.* **2015**, *21*, 15256 – 15262.
[40] P. Ferrari, J. Vanbuel, Y. Li, T.-W. Liao, E. Janssens, P. Lievens, *The Double-Laser Ablation Source Approach in Gas-Phase Synthesis of Nanoparticles* (Ed.: Y. Huttel), Wiley-VCH, Weinheim, **2017**, 59 – 78.
[41] S. M. Lang, P. Claes, S. Neukermans, E. Janssens, *J. Am. Soc. Mass Spectrom.* **2011**, *22*, 1508 – 1514.
[42] L. Drahos, V. Karoly, *J. Mass. Spectrom.* **2001**, *36*, 237 – 263.
[43] T. M. Bernhardt, J. Hagen, S. M. Lang, D. M. Popolan, L. D. Socaciu-Siebert, L. Wöste, *J. Phys. Chem. A* **2009**, *113*, 2724 – 2733.
[44] Y. Shao, Z. Gan, E. Epifanovsky, A. T. B. Gilbert, M. Wormit, J. Kussmann, A. W. Lange, A. Behn, J. Deng, X. Feng, D. Ghosh, M. Goldey, P. R. Horn, L. D. Jacobson, I. Kaliman, R. Z. Khaliullin, T. Kuś, A. Landau, J. Liu, E. I. Proynov, Y. M. Rhee, R. M. Richard, M. A. Rohrdanz, R. P. Steele, E. J. Sundstrom, H. L. Woodcock III, P. M. Zimmerman, D. Zuev, B. Albrecht, E. Alguire, B. Austin, G. J. O. Beran, Y. A. Bernard, E. Berquist, K. Brandhorst, K. B. Bravaya, S. T. Brown, D. Casanova, C.-M. Chang, Y. Chen, S. H. Chien, K. D. Closser, D. L. Crittenden, M. Diedenhofen, R. A. DiStasio Jr., H. Do, A. D. Dutoi, R. G. Edgar, S. Fatehi, L. Fusti-Molnar, A. Ghysels, A. Golubeva-Zadorozhnaya, J. Gomes, M. W. D. Hanson-Heine, P. H. P. Harbach, A. W. Hauser, E. G. Hohenstein, Z. C. Holden, T.-C. Jagau, H. Ji, B. Kaduk, K. Khistyaev, J. Kim, J. Kim, R. A. King, P. Klunzinger, D. Kosenkov, T. Kowalczyk, C. M. Krauter, K. U. Lao, A. D. Laurent, K. V. Lawler, S. V. Levchenko, C. Y. Lin, F. Liu, E. Livshits, R. C. Lochan, A. Luenser, P. Manohar, S. F. Manzer, S.-P. Mao, N. Mardirossian, A. V. Marenich, S. A. Maurer, N. J. Mayhall, E. Neuscamman, C. M. Oana, R. Olivares-Amaya, D. P. O'Neill, J. A. Parkhill, T. M. Perrine, R. Peverati, A. Prociuk, D. R. Rehn, E. Rosta, N. J. Russ, S. M. Sharada, S. Sharma, D. W. Small, A. Sodt, T. Stein, D. Stück, Y.-C. Su, A. J. W. Thom, T. Tsuchimochi, V. Vanovschi, L. Vogt, O. Vydrov, T. Wang, M. A. Watson, J. Wenzel, A. White, C. F. Williams, J. Yang, S. Yeganeh, S. R. Yost, Z.-Q. You, I. Y. Zhang, X. Zhang, Y. Zhao, B. R. Brooks, G. K. L. Chan, D. M. Chipman, C. J. Cramer, W. A. Goddard III, M. S. Gordon, W. J. Hehre, A. Klamt, H. F. Schaefer III, M. W. Schmidt,

C. D. Sherrill, D. G. Truhlar, A. Warshel, X. Xu, A. Aspuru-Guzik, R. Baer, A. T. Bell, N. A. Besley, J.-D. Chai, A. Dreuw, B. D. Dunietz, T. R. Furlani, S. R. Gwaltney, C.-P. Hsu, Y. Jung, J. Kong, D. S. Lambrecht, W. Liang, C. Ochsenfeld, V. A. Rassolov, L. V. Slipchenko, J. E. Subotnik, T. Van Voorhis, J. M. Herbert, A. I. Krylov, P. M. W. Gill, M. Head-Gordon, *Mol. Phys.* **2015**, *113*, 184 – 215.

[45] A. D. Becke, *Phys. Rev. A* **1988**, *38*, 3098 – 3100.
[46] J. P. Perdew, *Phys. Rev. B* **1986**, *33*, 8822 – 8824.
[47] T. H. Dunning, Jr., P. J. Hay in *Methods of Electronic Structure Theory, Vol. 2* (Ed.: H. F. Schaefer III), Plenum, New York, **1977**.
[48] P. J. Hay, W. R. Wadt, *J. Chem. Phys.* **1985**, *82*, 270 – 283.
[49] W. R. Wadt, P. J. Hay, *J. Chem. Phys.* **1985**, *82*, 284 – 298.
[50] P. J. Hay, W. R. Wadt, *J. Chem. Phys.* **1985**, *82*, 299 – 310.
[51] G. Zanti, D. Peeters, *Theor. Chem. Acc.* **2013**, *132*, 261 – 275.
[52] L. Lin, M. T. Nguyen, unpublished results.
[53] F. Liu, E. Proynov, J. G. Yu, T. R. Furlani, J. Kong, *J. Chem. Phys.* **2012**, *137*, 114104.
[54] F. Weigend, R. Ahlrichs, *Phys. Chem. Chem. Phys.* **2005**, *7*, 3297 – 3305.
[55] A. D. Becke, E. R. Johnson, *J. Chem. Phys.* **2005**, *122*, 154104.
[56] E. R. Johnson, A. D. Becke, *J. Chem. Phys.* **2005**, *123*, 024101.
[57] K. Raghavachari, G. W. Trucks, J. A. Pople, M. Head-Gordon, *Chem. Phys. Lett.* **1989**, *157*, 479 – 483.
[58] Z. Rolik, L. Szegedy, I. Ladjánszki, B. Ladóczki, M. Kállay, *J. Chem. Phys.* **2013**, *139*, 094105.
[59] P. R. Nagy, M. Kállay, *J. Chem. Phys.* **2017**, *146*, 214106.
[60] www.mrcc.hu.
[61] T. Yanai, D. Tew, N. Handy, *Chem. Phys. Lett.* **2004**, *393*, 51 – 57.
[62] S. Simon, M. Duran, J. J. Dannenberg, *J. Chem. Phys.* **1996**, *105*, 11024 – 11031.
[63] S. F. Boys, F. Bernardi, *Mol. Phys.* **1970**, *19*, 553 – 566.
[64] R. Z. Khaliullin, E. A. Cobar, R. C. Lochan, A. T. Bell, M. Head-Gordon, *J. Phys. Chem. A* **2007**, *111*, 8753 – 8765.
[65] H. Jacobsen, *Can. J. Chem.* **2008**, *86*, 695 – 702.
[66] H. L. Schmider, A. D. Becke, *J. Mol. Struct.* **2000**, *527*, 51 – 61.
[67] H. L. Schmider, A. D. Becke, *J. Chem. Phys.* **2002**, *116*, 3184 – 3193.
[68] R. F. W. Bader, *Atoms in Molecules*, Clarendon, Oxford, **1994**.
[69] NBO 6.0 E. D. Glendening, J. K. Badenhoop, A. E. Reed, J. E. Carpenter, J. A. Bohmann, C. M. Morales, C. R. Landis, F. Weinhold Theoretical Chemistry Institute, University of Wisconsin, Madison, **2013**.
[70] A. E. Reed, F. Weinhold, *J. Chem. Phys.* **1983**, *78*, 4066 – 4073.
[71] The PyMOL Molecular Graphics System, Version 1.7 Schrödinger, LLC.
[72] http://iqmol.org/.
[73] G. Schaftenaar, J. H. Noordik, *J. Comput. Aided Mol. Design* **2000**, *14*, 123 – 134.
[74] G. Schaftenaar, E. Vlieg, G. Vriend, *J. Comput. Aided Mol. Des.* **2017**, *31*, 789 – 800.
[75] T. Lu, F. Chen, *J. Comput. Chem.* **2012**, *33*, 580 – 592.
[76] P. Ferrari, L. M. Molina, V. E. Kaydashev, J. A. Alonso, P. Lievens, E. Janssens, *Angew. Chem. Int. Ed.* **2016**, *55*, 11059 – 11063; *Angew. Chem.* **2016**, *128*, 11225 – 11229.
[77] M. P. Johansson, I. Warnke, A. Le, F. Furche, *J. Phys. Chem. C* **2014**, *118*, 29370 – 29377.
[78] H. A. Hussein, J. B. A. Davis, R. L. Johnston, *Phys. Chem. Chem. Phys.* **2016**, *18*, 26133 – 26143.
[79] B. R. Goldsmith, J. Florian, J.-X. Liu, P. Gruene, J. T. Lyon, D. M. Rayner, A. Fielicke, M. Scheffler, L. M. Ghiringhelli, *Phys. Rev. Materials* **2019**, *3*, 016002.
[80] S. Chrétien, M. S. Gordon, H. Metiu, *J. Chem. Phys.* **2004**, *121*, 3756 – 3766.
[81] R. F. W. Bader, H. Essén, *J. Chem. Phys.* **1984**, *80*, 1943 – 1960.

Manuscript received: June 18, 2019
Revised manuscript received: September 8, 2019
Version of record online: November 7, 2019

